
⁸⁹Zr-Labeled High-Density Lipoprotein Nanoparticle PET Imaging Reveals Tumor Uptake in Patients with Esophageal Cancer

Kang H. Zheng¹, Jeffrey Kroon², Jasper Schoormans³, Oliver Gurney-Champion⁴, Sybren L. Meijer⁵, Suzanne S. Gisbertz⁶, Maarten C.C.M. Hulshof⁷, Danielle J. Vugts⁸, Guus A.M.S. van Dongen⁸, Bram F. Coolen³, Hein J. Verberne⁴, Aart J. Nederveen⁴, Erik S.G. Stroes¹, and Hanneke W.M. van Laarhoven⁹

¹Department of Vascular Medicine, Amsterdam Cardiovascular Sciences, Amsterdam UMC, University of Amsterdam, Amsterdam, The Netherlands; ²Department of Experimental Vascular Medicine, Amsterdam Cardiovascular Sciences, Amsterdam UMC, University of Amsterdam, Amsterdam, The Netherlands; ³Department of Biomedical Engineering and Physics, Amsterdam Cardiovascular Sciences, Amsterdam UMC, University of Amsterdam, Amsterdam, The Netherlands; ⁴Department of Radiology and Nuclear Medicine, Amsterdam UMC, University of Amsterdam, Amsterdam, The Netherlands; ⁵Department of Pathology, Cancer Center Amsterdam, Amsterdam UMC, University of Amsterdam, Amsterdam, The Netherlands; ⁶Department of Surgery, Cancer Center Amsterdam, Amsterdam UMC, University of Amsterdam, Amsterdam, The Netherlands; ⁷Department of Radiotherapy, Cancer Center Amsterdam, Amsterdam UMC, University of Amsterdam, Amsterdam, The Netherlands; ⁸Department of Radiology and Nuclear Medicine, Amsterdam UMC, VU University, Amsterdam, The Netherlands; and ⁹Department of Medical Oncology, Cancer Center Amsterdam, Amsterdam UMC, University of Amsterdam, Amsterdam, The Netherlands

Nanomedicine holds promise for the delivery of therapeutic and imaging agents to improve cancer treatment outcomes. Preclinical studies have demonstrated that high-density lipoprotein (HDL) nanoparticles accumulate in tumor tissue on intravenous administration. Whether this HDL-based nanomedicine concept is feasible in patients is unexplored. Using a multimodal imaging approach, we aimed to assess tumor uptake of exogenously administered HDL nanoparticles in patients with esophageal cancer. **Methods:** The HDL mimetic CER-001 was radiolabeled using ⁸⁹Zr to allow for PET/CT imaging. Patients with primary esophageal cancer staged T2 and above were recruited for serial ⁸⁹Zr-HDL PET/CT imaging before starting chemoradiation therapy. In addition, patients underwent routine ¹⁸F-FDG PET/CT and 3-T MRI scanning (diffusion-weighted imaging/intravoxel incoherent motion imaging and dynamic contrast-enhanced MRI) to assess tumor glucose metabolism, tumor cellularity and microcirculation perfusion, and tumor vascular permeability. Tumor biopsies were analyzed for the expression of HDL scavenger receptor class B1 and macrophage marker CD68 using immunofluorescence staining. **Results:** Nine patients with adenocarcinoma or squamous cell carcinoma underwent all study procedures. After injection of ⁸⁹Zr-HDL (39.2 ± 1.2 [mean ± SD] MBq), blood-pool SUV_{mean} decreased over time (11.0 ± 1.7, 6.5 ± 0.6, and 3.3 ± 0.5 at 1, 24, and 72 h, respectively), whereas liver and spleen SUV_{mean} remained relatively constant (4.1 ± 0.6, 4.0 ± 0.8, and 4.3 ± 0.8 at 1, 24, and 72 h, respectively, for the liver; 4.1 ± 0.3, 3.4 ± 0.3, and 3.1 ± 0.4 at 1, 24, and 72 h, respectively, for the spleen) and kidney SUV_{mean} markedly increased over time (4.1 ± 0.9, 9.3 ± 1.4, and 9.6 ± 2.0 at 1, 24, and 72 h, respectively). Tumor uptake (SUV_{peak}) increased over time (3.5 ± 1.1 and 5.5 ± 2.1 at 1 and 24 h, respectively [*P* = 0.016]; 5.7 ± 1.4 at 72 h [*P* = 0.001]). The effective dose of ⁸⁹Zr-HDL was 0.523 ± 0.040 mSv/MBq. No adverse events were observed after the administration of ⁸⁹Zr-HDL. PET/CT and 3-T MRI measures of tumor glucose metabolism,

tumor cellularity and microcirculation perfusion, and tumor vascular permeability did not correlate with tumor uptake of ⁸⁹Zr-HDL, suggesting that a specific mechanism mediated the accumulation of ⁸⁹Zr-HDL. Immunofluorescence staining of clinical biopsies demonstrated scavenger receptor class B1 and CD68 positivity in tumor tissue, establishing a potential cellular mechanism of action. **Conclusion:** To our knowledge, this was the first ⁸⁹Zr-HDL study in human oncology. ⁸⁹Zr-HDL PET/CT imaging demonstrated that intravenously administered HDL nanoparticles accumulated in tumors of patients with esophageal cancer. The administration of ⁸⁹Zr-HDL was safe. These findings may support the development of HDL nanoparticles as a clinical delivery platform for drug agents. ⁸⁹Zr-HDL imaging may guide drug development and serve as a biomarker for individualized therapy.

Key Words: zirconium; PET/CT; high-density lipoprotein; nanomedicine; esophageal cancer

J Nucl Med 2022; 63:1880–1886
DOI: 10.2967/jnumed.121.263330

Esophageal cancer is the sixth leading cause of death from cancer worldwide and represents a major health care problem (1). This malignancy is associated with substantial morbidity and has a dismal prognosis, with a 5-y survival rate of less than 25% (2), despite advances in multimodality treatment strategies. Oncologic treatment for esophageal carcinoma invariably involves the use of (pre-operative) chemotherapy or concurrent chemoradiation (3). An important limitation of systemic chemotherapy is nonspecificity, resulting in low intratumor drug concentrations, while off-target cytotoxic effects limit the intensity of dosing. Novel treatment strategies are needed to improve efficacy and avoid toxicity in the management of esophageal carcinoma.

Nanomedicine is an emerging approach to addressing the issues of poor outcomes and limited efficacy in oncology (4). The key principle involves the use of nanometer-sized particles as vehicles for drug or imaging agents to enhance delivery to tumors and avoid

Received Oct. 16, 2021; revision accepted Apr. 18, 2022.
For correspondence or reprints, contact Hanneke W.M. van Laarhoven (h.vanlaarhoven@amsterdamumc.nl).
Published online Jun. 23, 2022.
COPYRIGHT © 2022 by the Society of Nuclear Medicine and Molecular Imaging.

first-pass clearance by the liver. Compared with conventional therapies, such as systemic chemotherapy, nanoparticles should improve the balance between local efficacy and systemic toxicity. Several innovative nanomedicines have been approved by the U.S. Food and Drug Administration or reached the clinical stage of development (5). Nevertheless, clinical breakthroughs in terms of significantly prolonging patient survival have not yet been achieved by most nanoparticle platforms, comprising liposomes, albumin nanoparticles, or micelles. This situation may be due to inherent limitations of these nanosystems in dealing with the complexities and heterogeneity of tumor biology, including factors such as passive targeting, circulation half-life, tumor penetration, cellular uptake, and drug release. Specific toxicity associated with certain nanoparticles, such as hypersensitivity reactions, may also hamper clinical development (6).

High-density lipoproteins (HDLs) have received considerable interest because of their potential for drug delivery and imaging (7). HDLs are endogenous nanometer-sized particle carriers of cholesterol, and one of their main physiologic functions is considered to be the targeting and removal of cholesterol from peripheral tissues, including lipid-laden macrophages, followed by transportation to the liver for excretion (8). To exercise their function, HDLs have a natural conduit for interaction with peripheral cells through specific receptors, including scavenger receptor class B1 (SR-B1). HDLs can be formulated to carry, within their hydrophilic core or surface, therapeutic payloads, including hydrophobic drugs, controlled-released polymers, and short interfering RNAs (9). These characteristics and the absence of specific toxicity may allow HDLs to overcome the barriers to other nanosystems. In support of this notion, the administration of radiolabeled HDL nanoparticles in a mouse model of breast cancer resulted in accumulation in tumors through uptake in tumor-associated macrophages (10).

We aimed to investigate this concept in patients and set out to assess whether administered HDL nanoparticles accumulate in primary esophageal tumors. To this end, we labeled the HDL mimetic CER-001 with ^{89}Zr (^{89}Zr -HDL) to allow for in vivo tracing using serial PET/CT imaging (11). Furthermore, we explored whether tumor uptake of radiolabeled HDL was associated with tumor metabolism, as assessed with routine ^{18}F -FDG PET/CT; with tumor diffusion and microcirculation perfusion, as assessed with diffusion-weighted imaging/intravoxel incoherent motion imaging (DWI/IVIM); and with tumor vascular permeability, as assessed with dynamic contrast-enhanced MRI (DCE-MRI). Finally, we investigated the presence of the HDL receptor SR-B1 and macrophages in tumor biopsies using immunofluorescence.

MATERIALS AND METHODS

Study Design

This study was a single-center prospective trial and was conducted in accordance with the principles of the Declaration of Helsinki. The protocol was approved by the local ethics committee, and all participants provided written informed consent. Patients with esophageal cancer were included and visited the study center 3 times. All patients received a single injection of ^{89}Zr -HDL (CER-001; 10 mg; 37 MBq) and underwent serial PET/CT scanning at 1, 24, and 72 h after administration. In addition, all patients were scanned on a 3-T MRI scanner during 1 of the study visits.

Study Population

Eligible patients were adults with a primary esophageal carcinoma in situ before treatment, a histopathologically proven diagnosis, and a

tumor staged as at least locally advanced T2 (according to the TNM classification). Patients were recruited from the Gastro-Intestinal Oncology Center Amsterdam, Amsterdam, The Netherlands.

^{89}Zr -HDL and ^{18}F -FDG PET/CT

^{89}Zr -HDL was synthesized according to current good manufacturing practice guidelines. The procedure for ^{89}Zr radiolabeling of CER-001 and the quality and stability tests were described previously (11,12). The specific activity was 3.7 MBq of ^{89}Zr per mg of CER-001. Radiochemical purity was determined using size exclusion high-performance liquid chromatography ($100\% \pm 0\%$ [mean \pm SD]) and spin filters ($99.3\% \pm 0.4\%$). We demonstrated that covalent coupling of the bifunctional chelator *p*-isothiocyanatobenzyl desferrioxamine to CER-001 and subsequent labeling with zirconium did not affect its functionality in vitro and in vivo. Whole-body ^{89}Zr -HDL PET/CT scans were acquired on a Siemens Biograph mCT Flow system (Siemens). A low-dose CT scan was acquired with automatic modulation of current and voltage (reference values: 120 kV, 50 mA, 128×0.6 collimation, and 0.9 pitch). PET imaging was performed with continuous bed motion at 1.1 mm/s (legs) and 0.7 mm/s (body) in the 3-dimensional acquisition mode. CT data were used for PET attenuation correction, and PET data were reconstructed with the TrueX algorithm (3-dimensional ordered-subsets expectation maximization iterative reconstruction with time-of-flight and point spread function compensation, 21 subsets, 2 iterations, and a 5-mm gaussian postprocessing filter) in $4 \times 4 \times 5 \text{ mm}^3$ voxels.

^{18}F -FDG PET/CT scans were acquired in accordance with the local clinical protocol on the Siemens Biograph mCT Flow system. Patients were instructed to drink 2 L of water and to not perform strenuous physical activities in the 24 h preceding the scan. Patients fasted for at least 6 h, except for glucose-free oral hydration before the intravenous administration of ^{18}F -FDG. Fasting capillary blood glucose concentrations were measured with a blood glucose meter (StatStrip; Nova Biomedical Corp.) before ^{18}F -FDG administration. Dosages of ^{18}F -FDG ranged from 180 to 400 MBq, depending on the body mass index. PET/CT scanning was performed 60 min after the injection of ^{18}F -FDG. A diagnostic CT scan was acquired with automatic modulation of current and voltage (reference values: 120 kV, 160 mA, 128×0.6 collimation, and 0.9 pitch) after the intravenous administration of iodinated contrast medium (100 mL of Ultravist 300; Bayer Healthcare Pharmaceuticals) with a flow of 3 mL/s and a 65-s delay (portal phase). PET imaging was performed with continuous bed motion at 1.5 mm/s in the 3-dimensional acquisition mode. CT data were used for PET attenuation correction, and PET data were reconstructed with the TrueX algorithm (3-dimensional ordered-subsets expectation maximization iterative reconstruction with time-of-flight and point spread function compensation, 21 subsets, 2 iterations, and a 5-mm gaussian postprocessing filter) in $4 \times 4 \times 5 \text{ mm}^3$ voxels.

Image analysis was performed on a dedicated commercially available workstation (OsiriX [Pixmeo] and OLINDA/EXM [Hermes Medical Solutions]). Tumor uptake and organ uptake were assessed by manually drawing regions of interest delineating the whole tumor or organ (in all slices where visible) on the coregistered CT image. Blood-pool activity was determined by drawing regions of interest in 5 contiguous axial slices in the lumen of the superior vena cava. The SUV_{max} was calculated as the maximal pixel activity within each region of interest. For tumors, the SUV_{peak} was calculated as the mean pixel activity within a volume of interest (1 cm^3) centered around the hottest pixel value. The target-to-blood pool ratio was calculated by dividing the SUV by the mean blood-pool activity. The internal radiation dosimetry for the adult human was evaluated through the normalized cumulated activities for each patient, provided as input to the OLINDA/EXM code. Residence times were calculated for the liver, kidney, lungs, spleen, and remainder of the body by entering the percentage of the

TABLE 1
Baseline Characteristics of Included Patients

Patient	Age (y)	Sex	Body mass index (kg/m ²)	Tumor type	Tumor size (cm ³)	Tumor stage
1	73	M	26.7	Adenocarcinoma	20.4	T2N1M0
2	62	M	31.4	Adenocarcinoma	71.2	T3N1M0
3	68	M	19.4	Adenocarcinoma	16.2	T3N0M0
4	67	M	24.7	Squamous cell	97.3	T2N1M0
5	57	M	24.4	Adenocarcinoma	49.0	T3N2M1
6	66	M	26.1	Adenocarcinoma	53.7	T3N2M0
7	82	M	28.1	Adenocarcinoma	52.8	T3N1M0
8	51	M	28.1	Squamous cell	19.2	T3N2M0
9	66	M	30.4	Adenocarcinoma	52.8	T3N0M0

Tumors were classified according to TNM staging system.

injected dose at each time point for each patient in OLINDA/EXM and fitting these data using a monoexponential function.

3-T MRI Acquisition and Analysis

Patients were scanned on a 3-T MRI scanner (Philips Ingenia) with an anterior 16-channel phased-array coil and a posterior 16-channel phased-array coil. The maximum gradient strength of the scanner was 45 mT/m, and the maximum slew rate was 200 T/m/s. Three-dimensional T1-weighted 3-point Dixon and multislice T2-weighted turbo spin-echo images were obtained for reference.

DWI/IVIM. Axial diffusion-weighted 2-dimensional multislice single-shot echoplanar imaging with selective partial inversion recovery fat suppression was performed with the following acquisition settings: repetition time/echo time = 4600/70, field of view = 350 × 160 mm, resolution = 2.2 × 2.2 mm² (1.8 × 1.8 mm² reconstructed), number of slices = 20, slice thickness = 4.5 mm (slice gap = 0.5 mm), SENSE factor = 1.4, echoplanar imaging bandwidth = 16.5 Hz/voxel, and b values = 0 (3 averages), 100 (6 averages), and 800 (10 averages) s/mm². Scans were respiration triggered by means of a liver–lung interface navigator signal.

From the diffusion-weighted images, parameter maps were calculated for the diffusivity and perfusion fraction in MATLAB 2016a (The MathWorks, Inc.) on the basis of in-house software (13,14) adapted to work for 3 b values. Diffusivity was calculated voxelwise by applying a least-squares fit to the diffusion-weighted imaging data from the b values 100 and 800 s/mm²:

$$S(b) = S0' \times e^{-b \times D}, \quad \text{Eq. 1}$$

where $S(b)$ is the signal (S) at b value b and $S0'$ is the extrapolated signal at $b = 0$ s/mm² for monoexponential data. The difference between the measured S ($b = 0$ s/mm²) and $S0'$, in turn, relates to the perfusion fraction as:

$$f = 1 - \frac{S0'}{S(b=0)}. \quad \text{Eq. 2}$$

Regions of interest were drawn on $b = 800$ s/mm² and propagated to the parameter maps to assess parameter values inside the tumor regions.

DCE-MRI. For DCE-MRI, a highly accelerated golden-angle radial stack-of-stars TFE sequence (15) was performed continuously at a temporal resolution of 8.7 s per time frame. Two minutes after the start of the scan, a gadolinium-based contrast agent (Gadovist; Bayer) at a dose of 0.1 mmol/kg of body weight was injected intravenously at 2 mL/s.

Other relevant scan parameters were repetition time/echo time = 7.5/3.4, flip angle = 11°, and spatial resolution = 1 × 1 × 2 mm³.

The undersampled data were reconstructed in MATLAB 2016a using compressed sensing (ref) with total variation regularization in the time domain ($\lambda = 0.01$) and 100 iterations. Frame-by-frame tumor segmentation was performed on the dynamic data with ImageJ (National Institutes of Health). Signal intensity curves were obtained from the time series, and the area under the curve (AUC) was calculated for the first 2 min after contrast injection as a semiquantitative measure of tumor permeability.

Histology and Immunohistochemistry

Tumor biopsies were obtained during routine clinical workup before the start of neoadjuvant treatment and cut into slices. All samples were stained with hematoxylin and eosin for general morphology. For immunohistochemistry, the slides were dewaxed to remove the paraffin. Antigen retrieval was done using the LabVision PT module (ThermoFisher Scientific) at pH 6.0 for 20 min at 98°C. Next, the slides were washed with phosphate-buffered saline 3 times and blocked with Ultravision

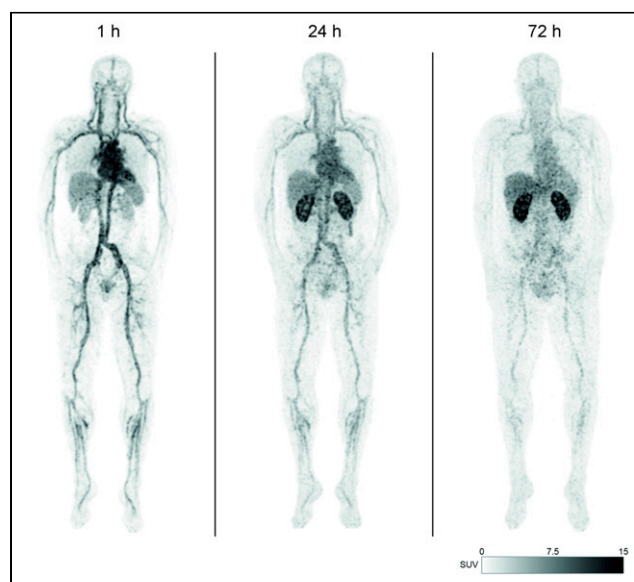


FIGURE 1. Maximum-intensity projections of serial ⁸⁹Zr-HDL PET images from patient 1.

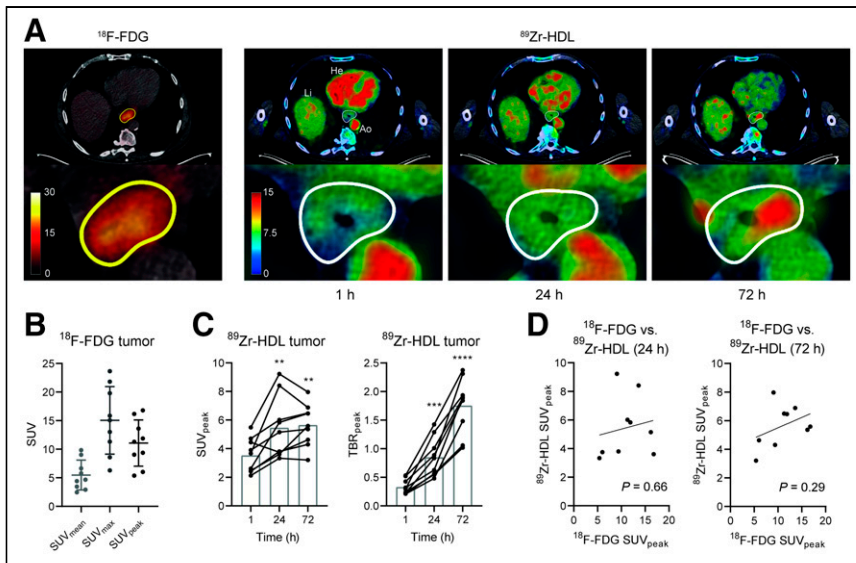


FIGURE 2. PET/CT images from patient 6 with esophageal adenocarcinoma. (A and B) ^{18}F -FDG uptake was clearly increased in tumors. On administration of ^{89}Zr -HDL, signal intensity in esophageal tumor increased over time, and focal uptake pattern was clearly visualized at 72 h. (C) Tumor SUVs and target-to-blood pool ratios increased over time, indicating accumulation of ^{89}Zr -HDL particles in tumors. (D) There was no association between ^{18}F -FDG uptake and ^{89}Zr -HDL uptake in tumors. Ao = aorta, He = heart, Li = liver; TBR = target-to-blood pool ratio.

protein block (TA-125-PBQ; ThermoFisher Scientific) for 10 min at room temperature. The slides were incubated with primary antibodies: for SR-B1, NB400-101 (Novus Biologicals), and for CD68, clone KP-1 (catalog number Ab955; Abcam). Subsequently, secondary antibodies Alexa Fluor-488 (A21121; Invitrogen) and Alexa Fluor-568 (A11036; Invitrogen) were used. Cells were embedded using Prolong-gold (P36935; ThermoFisher Scientific) containing 4,6-diamidino-2-phenylindole. Imaging was performed on a Leica DMI6000 (SP8) confocal microscope with a $\times 63$ objective. Pixels positive for either SR-B1 or CD68 per tumor biopsy were normalized for nuclear content using 4,6-diamidino-2-phenylindole to normalize the cellular biopsy area using Fiji (ImageJ v2.1.0/1.53c). The percentage of colocalization between SR-B1 and CD68 refers to the percentage of pixels from the total number of pixels per image and was determined using the Fiji Coloc 2 plugin.

Statistical Analysis

All data are presented as mean and SD. For the evaluation of ^{89}Zr -HDL uptake over time, a repeated-measures 1-way ANOVA was performed (significance level, $\alpha = 0.05$). If significance was found, then post hoc testing with Bonferroni adjustment was performed to assess the difference in uptake compared with the first time point. The correlations of ^{89}Zr -HDL uptake, MRI parameters, and immunohistochemistry data were tested using Pearson correlation coefficients. Statistical analyses were performed using SPSS Statistics package version 26 (IBM).

RESULTS

We recruited 9 male patients with a mean age of 66 ± 9 y; 7 (78%) of them were recently diagnosed with adenocarcinoma and 2 (22%) had squamous cell carcinoma of the esophagus. Baseline characteristics are listed in Table 1. All patients received an injection of 10 mg of ^{89}Zr -HDL (mean, 39.2 ± 1.2 MBq) and underwent serial PET/CT and 3-T MRI scanning before starting chemoradiation therapy. PET/CT scanning was performed at 1 h ($1 \text{ h } 3 \text{ min} \pm 0 \text{ h } 7 \text{ min}$), 24 h ($24 \text{ h } 41 \text{ min} \pm 0 \text{ h } 28 \text{ min}$), and 72 h

($71 \text{ h } 11 \text{ min} \pm 2 \text{ h } 6 \text{ min}$) after the injection of ^{89}Zr -HDL. ^{89}Zr -HDL was well tolerated during the study, and no adverse events were reported.

Biodistribution and Radiation Dosimetry of ^{89}Zr -HDL

Serial PET/CT imaging was performed at 1, 24, and 72 h after the injection of ^{89}Zr -HDL. Visual inspection revealed a clear radiotracer signal in the blood pool, liver, spleen, and kidneys (Fig. 1). The uptake of ^{89}Zr -HDL was measured in selected source organs (Supplemental Fig. 1) (supplemental materials are available at <http://jnm.snmjournals.org>). The blood-pool SUV_{mean} was 11.0 ± 1.7 at 1 h after administration and decreased to 6.5 ± 0.6 at 24 h and 3.3 ± 0.5 at 72 h (both P s < 0.0001). The liver SUV_{mean} was 4.1 ± 0.6 at 1 h and remained constant over time, whereas the spleen signal decreased slightly from 4.1 ± 0.3 to 3.4 ± 0.3 and 3.1 ± 0.4 after 24 and 72 h, respectively ($P < 0.001$). The kidney SUV_{mean} markedly increased from 4.1 ± 0.9 to 9.3 ± 1.4 after 24 h and remained elevated at 72 h ($P < 0.0001$), confirming

that the kidneys were the major site of catabolism of HDL. Organ dosimetry data and residence times are listed in Supplemental Table 1. The organs with the highest absorbed dose were the stomach (0.086 ± 0.013 mSv/MBq), lungs (0.070 ± 0.008 mSv/MBq), and liver (0.053 ± 0.010 mSv/MBq).

PET/CT Imaging of Esophageal Tumors

We used clinical ^{18}F -FDG PET/CT scans to assist in delineating the esophageal tumors; intense ^{18}F -FDG uptake was demonstrated, as expected (Figs. 2A and 2B). On colocalized ^{89}Zr -HDL PET/CT scans, focal uptake patterns in the esophageal tumors could clearly be observed from 24 h onward (Fig. 2A). Given the relatively small size of the esophageal tumors (mean, $48.0 \pm 26.6 \text{ cm}^3$) and the focal uptake patterns, tumor uptake of ^{89}Zr -HDL was reported using the SUV_{peak} for more robust quantification than the SUV_{max} . Tumor uptake of ^{89}Zr -HDL was significantly higher for all tumors at 24 and 72 h than at 1 h after injection (for SUV_{max} , 6.1 ± 1.4 and 9.2 ± 4.2 at 1 and 24 h, respectively [$P = 0.036$], and 10.2 ± 3.4 at 72 h [$P = 0.023$]; for SUV_{peak} , 3.5 ± 1.1 and 5.5 ± 2.1 at 1 and 24 h, respectively [$P = 0.016$], and 5.7 ± 1.4 at 72 h [$P = 0.001$]) (Fig. 2C). When corrected for the blood pool, the tumor target-to-blood pool ratio increased significantly over time (peak tumor-to-blood pool ratio, 0.3 ± 0.1 and 0.9 ± 0.3 at 1 and 24 h, respectively [$P < 0.001$], and 1.8 ± 0.5 at 72 h [$P < 0.001$]). There was no association between tumor uptake values for ^{18}F -FDG and ^{89}Zr -HDL (Fig. 2D).

DWI/IVIM and DCE-MRI of Esophageal Tumors

To explore whether characteristics of the tumor microenvironment affect the ability of HDL nanoparticles to penetrate tumors, all patients underwent DWI/IVIM and DCE-MRI scanning. We localized the tumors using T2-weighted turbo spin-echo images (Fig. 3A). DWI/IVIM images were acquired, and parameter maps of diffusivity and perfusion fraction were generated (Fig. 3B). The mean values for diffusivity and perfusion fraction of the tumors were not associated with tumor uptake of ^{89}Zr -HDL (Fig. 3C).

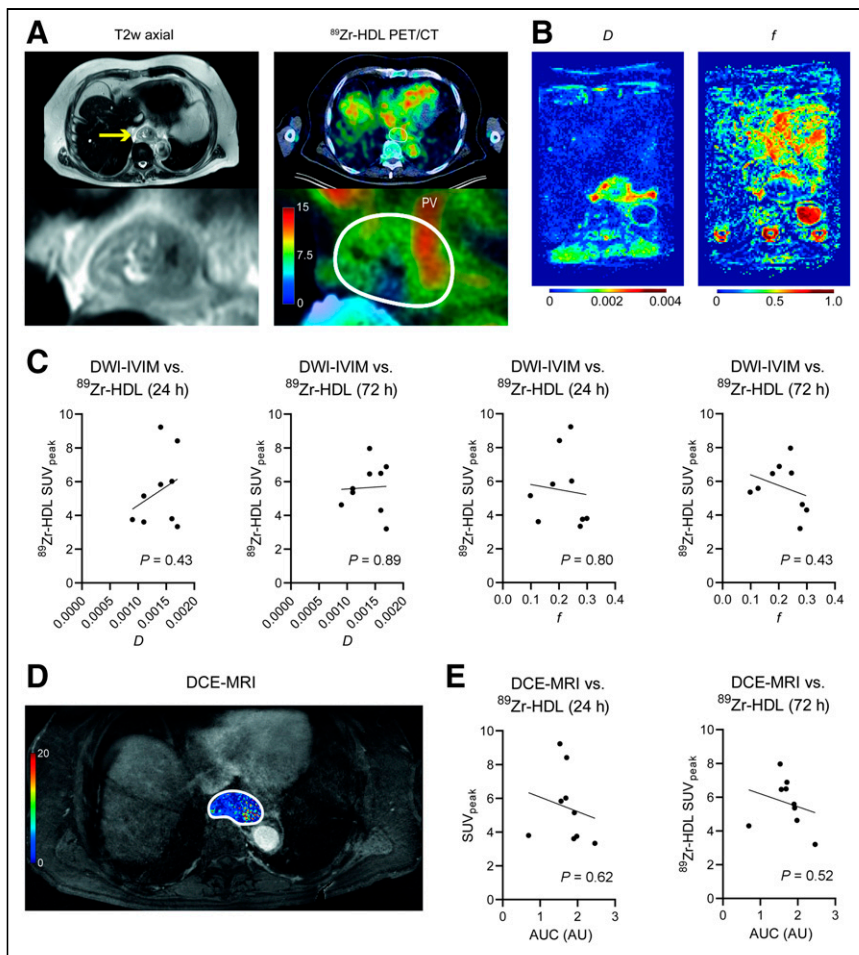


FIGURE 3. DWI/IVIM and DCE-MRI scanning of patient 7. (A) (Left) T2-weighted (T2w) turbo spin-echo images were obtained to localize tumors. Yellow arrow indicates tumor. (Right) Corresponding ^{89}Zr -HDL PET/CT at 72 h, with focal uptake in tumor delineated with white line, as well as intravascular signal from adjacent pulmonary vein (PV). (B) DWI/IVIM images were acquired to generate diffusivity (D) and perfusion fraction (f) maps. (C) Mean D and f values calculated from parameter maps were not associated with tumor uptake of ^{89}Zr -HDL. (D) Quantitative AUC maps resulting from DCE-MRI time series. (E) Mean AUC values were not associated with tumor uptake of ^{89}Zr -HDL. AU = arbitrary units.

DCE-MRI time series were obtained, and quantitative pixelwise AUC maps were calculated from the first 2 min after the injection of a gadolinium-based contrast agent (Fig. 3D). The mean AUC values of the tumors, as a measure of permeability, were not associated with tumor uptake of ^{89}Zr -HDL (Fig. 3E).

HDL Receptor Expression in Tumor Biopsies

Histologic analysis of tumor biopsies from all patients was performed to assess general morphology (Fig. 4A), the expression of the HDL receptor SR-B1, and the presence of macrophage marker CD68 (Fig. 4B). We established and quantified the presence of SR-B1-positive cells and macrophages by CD68 expression (Fig. 4C) as well as cells with double positivity for these markers (Fig. 4D). There was no relationship between semiquantitative measures of SR-B1 and CD68 expression and tumor uptake of ^{89}Zr -HDL (Supplemental Fig. 2).

DISCUSSION

To our knowledge, this is the first report of the uptake of HDL nanoparticles in tumors of patients with primary esophageal

cancer. After the administration of ^{89}Zr -HDL, serial PET/CT demonstrated the accumulation of HDL nanoparticles in the esophageal tumors over time. Tumor uptake could be quantified in all patients, and no adverse events occurred. These findings herald the clinical utility of HDL-based nanomedicine to target esophageal tumors for the delivery of anticancer drugs.

In this proof-of-concept study, we applied ^{89}Zr labeling to the HDL mimetic CER-001, which consists of recombinant apolipoprotein A-I and phospholipids. Our data indicated relatively low uptake in the liver and spleen, whereas the radiotracer signal increased in the kidneys over time. This finding is in line with the known renal catabolism of apolipoprotein A-I (16). Importantly, focal accumulation patterns of ^{89}Zr -HDL were observed in all esophageal tumors after 24 and 72 h. These data highlight the translational potential of HDL nanoparticles as a tool for altering the biodistribution of drugs of interest, to achieve higher intratumor concentrations, and to avoid systemic toxicity. This concept is supported by previous experimental studies in cardiovascular disease, which established that HDL nanoparticles effectively delivered their drug payload to atherosclerotic plaques (17,18).

The extravasation of nanoparticles to tumors is traditionally considered to depend on passive accumulation via the enhanced permeability and retention (EPR) effect (19). This phenomenon dictates that drug penetration in tumors is dependent on features of the tumor microenvironment, including the degree of cellularity and composition of the extracellular matrix, as well as vascular permeability. Nevertheless, we found that tumor uptake of ^{89}Zr -HDL was not associated with imaging measures of tumor diffusivity (DWI/IVIM), tumor perfusion (DWI/IVIM), or vascular permeability (DCE-MRI). These findings suggest the contribution of a specific mechanism mediating the accumulation of HDL nanoparticles in esophageal cancer, rather than dependence on only passive vascular leakage.

We substantiated the presence of the HDL receptor SR-B1 in tumor biopsies from the studied patients—which could facilitate a specific mechanism for the accumulation of HDL. Enhanced expression of SR-B1 has been suggested to be a mechanism for tumor cells to satisfy their increased demand for cholesterol to allow for proliferation and increased metabolic cellular processes (20). The level of SR-B1 expression in human breast and prostate cancers is associated with tumor aggressiveness and adverse prognosis (21,22), and a variety of malignant cell lines overexpress SR-B1 (20). Yet, we did not find an association between tumor uptake of ^{89}Zr -HDL and tumor glycolytic activity (related to cellular proliferation), as measured with ^{18}F -FDG PET/CT. Prior studies using murine breast cancer models suggested that injected HDL nanoparticles are preferentially taken up by tumor-associated

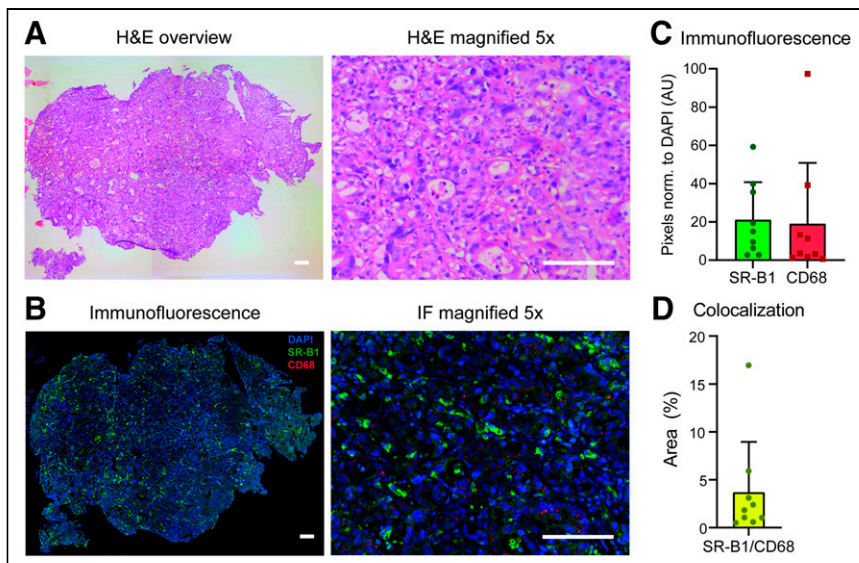


FIGURE 4. HDL receptor expression and macrophage presence in tumor biopsies, as shown by histology and immunofluorescence (IF) of tumor biopsies before chemoradiation therapy, in patient 3. (A and B) Hematoxylin and eosin (H&E) staining (A) with corresponding confocal microscopy image for 4,6-diamidino-2-phenylindole (DAPI) (blue), SR-B1 (green), and CD68 (red) (B). (C) Pixel count of SR-B1 and CD68 normalized (norm.) to DAPI. (D) Percentage area with double positivity for SR-B1 and CD68. AU = arbitrary units.

macrophages (10,23), which may also express SR-B1 or other scavenger receptors for HDL. However, we found that the colocalization of SR-B1 with CD68 was limited, suggesting that cells other than macrophages could be responsible for most uptake of HDL particles. Additional studies are needed to assess the cellular distribution of administered HDL particles in patients with esophageal cancer, as well as the cellular mechanisms involved. Collectively, ^{89}Zr -HDL PET/CT has the potential to serve as a specific imaging biomarker for predicting the efficacy of HDL-mediated drug delivery (24).

To our knowledge, this is the first report of the radiation dosimetry of ^{89}Zr -HDL. The effective dose of ^{89}Zr -HDL (0.523 mSv/MBq) clearly exceeds that of the conventional diagnostic tracer ^{18}F -FDG (0.019 mSv/MBq) (25), although it is comparable to those of other ^{89}Zr -immuno-PET tracers (26). Although this dose may limit repetitive use, given the poor survival rate of patients with esophageal cancer, the risks of radiation may be acceptable when weighed against any potential future improvement in clinical treatment provided by this imaging modality.

We acknowledge several limitations of the present study. The sample size was small for a pilot study and carries the risk of a false-negative finding in our correlation testing of imaging modalities. The spatial heterogeneity of the tumors may have obscured MRI parameters that were calculated by averaging measurements in a region of interest. Finally, biopsies of tumors may not adequately reflect the tissue distribution of the tumors.

CONCLUSION

^{89}Zr labeling of HDL nanoparticles allowed for in vivo tracing using PET/CT in patients with esophageal cancer. The administration of ^{89}Zr -HDL was safe, and the effective dose was in the range of those of other ^{89}Zr tracers. Focal uptake patterns were observed within the esophageal tumors. Further studies are now needed to gain insight into the mechanisms of HDL accumulation in tumors

and to test the feasibility of HDL nanoparticles serving as a delivery system for anti-cancer drugs.

DISCLOSURE

This work was supported by the Dutch Heart Foundation (CVON 2017–20: GENIUS-II). Jeffrey Kroon was supported by Dutch Heart Foundation Senior Scientist Dekker Grant 2021T045. This was an investigator-initiated study for which Cerenis provided CER-001. Erik S.G. Stroos also served as principal investigator for the MODE, SAMBA, and TANGO studies (involving CER-001). No other potential conflict of interest relevant to this article was reported.

ACKNOWLEDGMENTS

We thank E. Poel, M.F. Lam, and S.R. Havik for their invaluable technical assistance.

KEY POINTS

QUESTION: Do intravenously administered HDL nanoparticles accumulate in tumors in patients with primary esophageal cancer?

PERTINENT FINDINGS: This prospective imaging study used ^{89}Zr labeling of HDL nanoparticles to demonstrate accumulation in tumors of patients with esophageal cancer after intravenous administration (SUV_{peak} : 3.5 ± 1.1 , 5.5 ± 2.1 , and 5.7 ± 1.4 at 1, 24, and 72 h, respectively). Tumor uptake of ^{89}Zr -HDL was not associated with measures from ^{18}F -FDG PET/CT, DWI/IVIM, and DCE-MRI, suggesting that a specific mechanism mediated the accumulation of ^{89}Zr -HDL; analysis of tumor biopsies showed the presence of SR-B1–positive cells and macrophages, indicating a potential mechanism of action.

IMPLICATIONS FOR PATIENT CARE: HDL nanoparticles have the potential to serve as a delivery system for anticancer drugs in esophageal cancer.

REFERENCES

- Smyth EC, Lagergren J, Fitzgerald RC, et al. Oesophageal cancer. *Nat Rev Dis Primers*. 2017;3:17048.
- van Putten M, de Vos-Geelen J, Nieuwenhuijzen GAP, et al. Long-term survival improvement in oesophageal cancer in the Netherlands. *Eur J Cancer*. 2018;94:138–147.
- Shah MA, Kennedy EB, Catenacci DV, et al. Treatment of locally advanced esophageal carcinoma: ASCO guideline. *J Clin Oncol*. 2020;38:2677–2694.
- Shi J, Kantoff PW, Wooster R, Farokhzad OC. Cancer nanomedicine: progress, challenges and opportunities. *Nat Rev Cancer*. 2017;17:20–37.
- Tran S, DeGiovanni P-J, Piel B, Rai P. Cancer nanomedicine: a review of recent success in drug delivery. *Clin Transl Med*. 2017;6:44.
- Szebeni J, Simberg D, Gonzalez-Fernandez A, Barenholz Y, Dobrovolskaia MA. Roadmap and strategy for overcoming infusion reactions to nanomedicines. *Nat Nanotechnol*. 2018;13:1100–1108.
- Lobatto ME, Fuster V, Fayad ZA, Mulder WJ. Perspectives and opportunities for nanomedicine in the management of atherosclerosis. *Nat Rev Drug Discov*. 2011;10:835–852.

8. Ouimet M, Barrett TJ, Fisher EA. HDL and reverse cholesterol transport. *Circ Res*. 2019;124:1505–1518.
9. Mulder WJM, van Leent MMT, Lameijer M, Fisher EA, Fayad ZA, Perez-Medina C. High-density lipoprotein nanobiologics for precision medicine. *Acc Chem Res*. 2018;51:127–137.
10. Pérez-Medina C, Tang J, Abdel-Atti D, et al. PET imaging of tumor-associated macrophages with ⁸⁹Zr-labeled high-density lipoprotein nanoparticles. *J Nucl Med*. 2015;56:1272–1277.
11. Zheng KH, van der Valk FM, Smits LP, et al. HDL mimetic CER-001 targets atherosclerotic plaques in patients. *Atherosclerosis*. 2016;251:381–388.
12. Vosjan MJ, Perk LR, Visser GW, et al. Conjugation and radiolabeling of monoclonal antibodies with zirconium-89 for PET imaging using the bifunctional chelate *p*-isothiocyanatobenzyl-desferrioxamine. *Nat Protoc*. 2010;5:739–743.
13. Gurney-Champion OJ, Froeling M, Klaassen R, et al. Minimizing the acquisition time for intravoxel incoherent motion magnetic resonance imaging acquisitions in the liver and pancreas. *Invest Radiol*. 2016;51:211–220.
14. Klaassen R, Gurney-Champion OJ, Engelbrecht MRW, et al. Evaluation of six diffusion-weighted MRI models for assessing effects of neoadjuvant chemoradiation in pancreatic cancer patients. *Int J Radiat Oncol Biol Phys*. 2018;102:1052–1062.
15. Zheng KH, Schoormans J, Stiekema LCA, et al. Plaque permeability assessed with DCE-MRI associates with USPIO uptake in patients with peripheral artery disease. *JACC Cardiovasc Imaging*. 2019;12:2081–2083.
16. Moestrup SK, Nielsen LB. The role of the kidney in lipid metabolism. *Curr Opin Lipidol*. 2005;16:301–306.
17. Duivenvoorden R, Tang J, Cormode DP, et al. A statin-loaded reconstituted high-density lipoprotein nanoparticle inhibits atherosclerotic plaque inflammation. *Nat Commun*. 2014;5:3065.
18. Kim Y, Lobatto ME, Kawahara T, et al. Probing nanoparticle translocation across the permeable endothelium in experimental atherosclerosis. *Proc Natl Acad Sci USA*. 2014;111:1078–1083.
19. Prabhakar U, Maeda H, Jain RK, et al. Challenges and key considerations of the enhanced permeability and retention effect for nanomedicine drug delivery in oncology. *Cancer Res*. 2013;73:2412–2417.
20. Mooberry LK, Sabnis NA, Panchoo M, Nagarajan B, Lacko AG. Targeting the SR-B1 receptor as a gateway for cancer therapy and imaging. *Front Pharmacol*. 2016;7:466.
21. Schörghofer D, Kinslechner K, Preitschopf A, et al. The HDL receptor SR-B1 is associated with human prostate cancer progression and plays a possible role in establishing androgen independence. *Reprod Biol Endocrinol*. 2015;13:88.
22. Yuan B, Wu C, Wang X, et al. High scavenger receptor class B type I expression is related to tumor aggressiveness and poor prognosis in breast cancer. *Tumour Biol*. 2016;37:3581–3588.
23. Mason CA, Kossatz S, Carter LM, et al. An ⁸⁹Zr-HDL PET tracer monitors response to a CSF1R inhibitor. *J Nucl Med*. 2020;61:433–436.
24. Jauw YWS, Willemien Menke-van der Houven van Oordt C, Hoekstra OS, et al. Immuno-positron emission tomography with zirconium-89-labeled monoclonal antibodies in oncology: what can we learn from initial clinical trials? *Front Pharmacol*. 2016;7:131.
25. Mattsson S, Johansson L, Leide Svegborn S, et al. Radiation dose to patients from radiopharmaceuticals: a compendium of current information related to frequently used substances. *Ann ICRP*. 2015;44(2 suppl):7–321.
26. Börjesson PK, Jauw YW, de Bree R, et al. Radiation dosimetry of ⁸⁹Zr-labeled chimeric monoclonal antibody U36 as used for immuno-PET in head and neck cancer patients. *J Nucl Med*. 2009;50:1828–1836.